

# Global Probes of the Impact of Baryons on Dark Matter Halos

C.S. Kochanek and Martin White

Harvard-Smithsonian Center for Astrophysics, 60 Garden St., Cambridge, MA 02138

email: ckochanek, mwhite@cfa.harvard.edu

## ABSTRACT

The halo mass function,  $dn/dM$ , predicted by hierarchical clustering models can be measured indirectly using dynamical probes like the distribution of gravitational lens image separations,  $dn/d\Delta\theta$ , or halo circular velocities,  $dn/dv_c$ . These dynamical variables depend on the halo structure as well as the halo mass. Since baryonic physics, particularly cooling, significantly modifies the central density structure of dark matter halos, both observational distributions show a feature corresponding to the mass scale below which the baryons in the halo can cool (i.e. galaxies versus clusters). We use simplified but self-consistent models to show that the structural changes to the halos produced by the cooling baryons explain both distributions. Given a fixed halo mass function, matching the observed image separation distribution or local velocity function depends largely on  $\Omega_b$  through its effects on the cooling time scales. These baryonic effects on the halo structure also affect the evolution of the velocity function of galaxies with redshift.

*Subject headings:* cosmology: theory – galaxies: formation – gravitational lensing – large-scale structure of universe – dark matter

## 1. Introduction

The number density, spatial distribution and properties of dark matter halos are now well understood in models based on hierarchical clustering (e.g. Jenkins et al. 2000; Sheth & Tormen 1999; Navarro, Frenk & White 1996; Moore et al. 1998), thanks in large part to numerical experiments involving high resolution N-body simulations. However, the relationship between these dark matter halos and astrophysical objects can be complicated by the modifications to the halos produced by baryonic physics and the dependence of our search and measurement methods on their baryonic properties. The dominant divide in the observed properties of halos is between galaxies and groups or clusters of galaxies. Physically this division is between halos in which the baryons have cooled and formed stars as compared to halos which have not (Silk 1977; Rees & Ostriker 1977; White & Rees 1978; Blumenthal et al. 1984).

In this paper we explore how the halo mass function,  $dn/dM$ , is globally related to the masses or internal velocities of the objects we observe. By using dynamical probes of the halos

rather than luminosities we can try to avoid two problems. First, dynamical probes can provide a common measurement scale for both galaxies and clusters, allowing us to explore the location and properties of the boundary between the two types of astronomical objects. Second, by focusing on dynamical properties of the halos rather than luminosities, we partly avoid the issues related to star formation and feedback which are central to any relationship between the halo mass function and the luminosity function,  $dn/dL$ .

We cannot, however, simply ignore the effects of the baryons, because the baryons significantly modify the halo structure when they cool (e.g Blumenthal et al. 1986; Mo, Mao & White 1998; Cole et al. 2000; Gonzalez et al. 2000). Both massive galaxies and small groups of galaxies can have internal velocity dispersions  $\sim 200 \text{ km s}^{-1}$ , but it is difficult to infer from that fact the total, and presumably different, masses of the two systems. Thus, any global relationship between the halo mass function,  $dn/dM$ , and the observed properties of galaxies, groups and clusters should show a feature at the cooling mass scale  $M_c$  dividing cooled and uncooled halos. In this paper we quantitatively develop this theme by combining Press-Schechter (1974) based estimates of the mass function with adiabatic compression models (e.g. Blumenthal et al. 1986) to estimate the effects of the cooling baryons on the structure of the halo. This allows us to make relatively self-consistent estimates for the effects of the baryons in distorting the initial halo mass function into what our observational probes can measure.

Many of the issues we will explore have been treated in earlier studies. That differences in cooling time scales create the division between galaxies and clusters is well known, and most of the effects we discuss are explicitly included in semi-analytic models<sup>1</sup> of galaxy formation (e.g. Lacey & Silk 1991; White & Frenk 1991; Cole et al. 1994; Baugh, Cole & Frenk 1996; Kauffman, White & Guiderdoni 1993; Kauffman et al. 1999; Somerville & Primack 1999; Benson et al. 2000; Cole et al. 2000). However our focus here is somewhat different and we highlight two issues which have not previously been emphasized. First, we focus on global probes of the mass function on both galaxy and cluster scales and the role of cooling in producing a measurable feature in these observational distributions. Second, we emphasize the importance of structural changes in the mass distribution of the dark matter halo rather than the effects of cooling on the star formation rate and luminosity/colors of galaxies which are a major focus of semi-analytic work.

The outline of the paper is as follows. In §2 we review the modified Press-Schechter formalism which we use for determining the mass function of halos, adiabatic compression models for the effects of the cooling baryons on the structure of the halos, and simple cooling models for the determining the cooling mass scale. In §3 we use these models to explore the distribution of image separations in gravitational lenses, and in §4 we illustrate the effects of the cooling baryons on the distribution of halos in dynamical velocities. In §5 we summarize our results.

---

<sup>1</sup>Since the cooling models adopted in the current generation of semi-analytic models are very similar, we will collectively refer to them as “SA” hereafter

## 2. The Properties of Halos

Our models have three elements. First, we need to estimate the mass function of halos,  $dn/dM$ , and the formation epoch of each halo. Second, we need to estimate how the structure of the halo is modified by the cooling of the baryons. Third, we need to estimate whether the baryons in the halo have cooled. We will use a fixed cosmological model throughout the paper, the so-called “concordance” model of Ostriker & Steinhardt (1995) which provides an acceptable fit to a wide range of current observations. This is a  $\Lambda$ CDM model with a matter density (in units of the critical density)  $\Omega_m = 0.3$ , a Hubble constant  $H_0 = 67 \text{ km s}^{-1} \text{ Mpc}^{-1}$ , and a baryon density  $\Omega_b = 0.04$  normalized to match the abundance of rich clusters of galaxies ( $\sigma_8 = 0.9$ ).

### 2.1. The Halo Mass Function and Formation Time

To calculate the cosmological mass function of dark matter halos we use a fit to the results of the Virgo simulations (Sheth & Tormen 1999; Jenkins et al. 2000). We assign halos of mass  $M$  to peaks of height  $\nu$

$$\nu \equiv \left( \frac{\delta_c}{\sigma(M)} \right)^2 \quad (1)$$

where  $\delta_c = 1.69$  and  $\sigma(M)$  is the rms fluctuation in the matter density smoothed with a top-hat filter on a scale  $R^3 = 3M/4\pi\bar{\rho}$  with  $\bar{\rho}$  the mean matter density. Press-Schechter (1974) theory postulates that the mass function can be cast in terms of  $\nu$  into a universal form

$$\frac{M}{\bar{\rho}} \frac{dn}{dM} dM = f(\nu) d\nu \quad (2)$$

where  $f(\nu)$  is known as the multiplicity function. We use<sup>2</sup> (Sheth & Tormen 1999)

$$\nu f(\nu) = A(1 + \nu'^{-p})\nu'^{1/2}e^{-\nu'/2} \quad (3)$$

where  $p = 0.3$  and  $\nu' = 0.707\nu$ . The normalization constant  $A$  is fixed by the requirement that all of the mass lie in a given halo

$$\int f(\nu) d\nu = 1 \quad . \quad (4)$$

The Press-Schechter form is given by  $p \rightarrow 0$  and  $\nu' \rightarrow \nu$ .

Later we will need to know the distribution of formation times for our dark matter halos. Following Kitayama & Suto (1996) and Newman & Davis (2000) we model the formation time distribution using the extended Press-Schechter theory outlined in Lacey & Cole (1994). The formation time distribution,  $dp/dt_{\text{form}}$ , is an integral over mass of the progenitors which merge

---

<sup>2</sup>We use this form rather than the fit from Jenkins et al. (2000) because the range of validity of the latter is too small for our purposes.

to form a given halo at the observed redshift (Lacey & Cole 1994; Eq. 2.19). Because this integral can be difficult to evaluate numerically we in fact integrate the cumulative probability distribution and obtain the desired differential distribution by finite difference. Since all of the time dependence is in the threshold parameters  $\delta(t)$  this can be cast into an elegant form and is very stable numerically.

## 2.2. Adiabatic Compression

The dark matter halo number densities calculated above represent “primordial” halos. To make contact with observations it is necessary to take into account the effects of baryons on halo structure and dynamics. We follow Mo et al. (1998) in estimating the modifications in the mass distribution of the halos created by the cooling baryons, though similar approaches are used by Dalcanton, Spergel & Summers (1997), Cole et al. (2000) and Gonzalez et al. (2000).

We assume that the halos all have spherical profiles depending only on the mass and we neglect any substructure or halos-within-halos. Specifically we model the profile with the “universal” form<sup>3</sup> described by Navarro, Frenk & White (1996; hereafter NFW)

$$\rho(r) \propto \frac{1}{x(1+x)^2} \quad (5)$$

where  $x = r/r_s$  is the radius measured in units of a characteristic scale  $r_s$ . Each halo can then be characterized by two numbers. Rather than  $r_s$  and the constant of proportionality in Eq. (5), we take these to be the virial mass and the concentration. The virial mass  $M_{\text{vir}}$  is the total mass inside the virial radius  $r_{\text{vir}}$ : the radius within which the mean density exceeds the critical density by a factor of  $\Delta_c(z)$ . In an Einstein-de Sitter model  $\Delta_c = 18\pi^2 \simeq 178$ . It is lower for  $\Omega_m < 1$ , taking the value  $\Delta_c \simeq 100$  for the “concordance” cosmology. We estimated the concentration of the halos,

$$c \equiv \frac{r_{\text{vir}}}{r_s} = \frac{9}{1+z} \left( \frac{M_{\text{vir}}}{8.12 \times 10^{12} M_{\odot}} \right)^{-0.14}, \quad (6)$$

using the average relation found by Bullock et al. (2000; see also Eke, Navarro & Steinmetz 2001). Physically this suggests that  $r_s$  is roughly constant with redshift. Finally, the halo is assumed to have angular momentum  $J$  specified by its spin parameter  $\lambda = J|E|^{1/2}/GM_{\text{vir}}^{5/2}$ , where the binding energy  $|E|$  is computed using the virial theorem.

We model the disk of the galaxy as an exponential disk characterized by mass  $M_d = m_d M_{\text{vir}}$  and scale length  $r_d$ . The disk is assumed to have angular momentum  $J_d = j_d J$ , and this is used to determine the disk scale length. If  $j_d = m_d$ , the specific angular momentum of the disk is the same as that of the halo. Unlike Mo et al. (1998), who considered adding a bulge component as

---

<sup>3</sup>Our results will not depend sensitively on this choice. The alternate form of Moore et al. (1998) would work just as well.

a point mass, we added a bulge modeled as a Hernquist (1990) profile with mass  $M_b = m_b M_{\text{vir}}$  and a Hernquist scale length  $a_b$ . In contrast to the disk, there is no conserved quantity like the angular momentum that can be used to determine the bulge scale length. Instead we simply used a phenomenological scaling<sup>4</sup> that  $a = 0.045 r_d$ . We assumed that the total specific angular momentum of the baryons was the same as the dark matter, but that all of the angular momentum is in the disk component ( $j_d = m_d + m_b$ ) while the bulge has none.

The dark matter is adiabatically compressed by the cooled baryons, which for a spherical system of particles on circular orbits means conserving the mass and angular momentum (e.g. Blumenthal et al. 1986). Thus, a dark matter particle initially orbiting at radius  $r_i$  ends up at radius  $r$  where  $r_i M_i(r_i) = r M_f(r)$  and  $M_i(r_i)$  and  $M_f(r)$  are the initial and final mass distributions. The initial mass distribution is simply that of the NFW halo,  $M_{\text{NFW}}(r_i)$ , while the final mass distribution is

$$M_f(r) = M_d(r) + M_b(r) + (1 - m_d - m_b) M_{\text{NFW}}(r_i). \quad (7)$$

After making an initial estimate for the disk scale length,  $M_f(r)$  is found by iteratively solving Eq. (7) while adjusting the disk and bulge scale lengths to satisfy the disk angular momentum constraint (see Mo et al. 1998)

$$J_d = j_d J = 2\pi \int_0^{r_{\text{vir}}} R dR v_c(R) R \Sigma(R) \quad (8)$$

where  $v_c(R)$  is the rotation curve in the disk and  $\Sigma(R)$  is the surface mass density of the disk. The rotation curve  $v_c(R)$  is computed assuming that the bulge and the halo remain spherical while the disk is an infinitely thin exponential disk.

### 2.3. A Very Simple Cooling Model

We treat cooling using two very simple models. The first is simply adding a cooling mass scale  $M_c$  by hand. We assume that the probability that a halo has cooled is given by

$$P_{\text{cool}}(M) = 1 - \left[ 1 + \exp\left(\frac{\log M - \log M_c}{\Delta M_c}\right) \right]^{-1} \quad (9)$$

with a cooling mass scale  $M_c$  and an (arbitrary!) logarithmic distribution width of  $\Delta M_c = 0.1$  to smooth the transition. Half of the halos with  $M = M_c$  have cooled, and the total distribution of halos is the sum of the cooled and uncooled distributions. For any observational test we can vary the cooling mass scale  $M_c$  until we achieve a reasonable match.

---

<sup>4</sup>In the photometric survey of spiral galaxies by de Jong (1996), bulge effective radii are typically  $R_e \simeq r_d/10$  of the disk scale length  $r_d$ , with a logarithmic scatter of 0.17 dex. For a Hernquist model, the scale length is  $a = 0.45 R_e$  of a de Vaucouleurs effective radius  $R_e$ , so we use  $a = 0.045 r_d$ .

The second model is based on a simplified version of the cooling model used by Cole et al. (2000) in their semi-analytic models of galaxy formation. We will use this model both to check whether our estimate of the cooling mass scale (§3.3.1) is reasonable and as a complete self-consistent model (§3.3.2). As we are interested only in the boundary between galaxies and clusters, we neglect the complicated details of star formation and feedback and consider only cooled mass fractions. We assume that when the halo collapses, the gas is heated to the virial temperature  $k_B T_{\text{vir}} = \frac{1}{2} \mu m_p v_{\text{vir}}^2$  where  $m_p$  is the proton mass and  $\mu$  is the mean molecular weight. We assume that the initial density distribution of the gas is  $\rho_{\text{gas}} \propto (r^2 + r_c^2)^{-1}$  for  $r < r_{\text{vir}}$  where  $r_c = r_s/3$ . This is the phenomenological model which Cole et al. (2000) develop based on more realistic collapse simulations with hydrodynamics. Given the temperature, the gas density and the Sutherland & Dopita (1986) cooling curves, we can estimate the cooling time as a function of radius,

$$\tau_{\text{cool}}(r) = \frac{3\mu^2 m_p^2 v_{\text{vir}}^2}{4\rho_{\text{gas}} \Lambda_N(T_{\text{vir}})} \quad (10)$$

where we have fixed the metallicity to  $Z = Z_{\odot}/3$  for simplicity.

As a consistency check, we can estimate the age of a halo and the time for a given fraction of the baryons to cool to see if they match at a mass scale comparable to our estimated cooling mass scale  $M_c$  (§3.3.1). We can also use the cooling model to determine the cooled baryon fraction of each halo. Given the average age,  $t_{\text{form}}(M, z)$ , for halos of mass  $M$  and redshift  $z$ , we calculate the cooled baryonic mass fraction  $f_{\text{cool}}(M, z)$  by the mass fraction inside the radius where the cooling time equals the age,  $t(z) - t_{\text{form}}(M, z) = \tau_{\text{cool}}(r_{\text{cool}})$ . If the global baryon fraction is  $(m_d + m_b)_0$ , then we model the halo with an adiabatic compression model having a baryon fraction  $m_d + m_b = f_{\text{cool}}(M, z)(m_d + m_b)_0$ , eliminating the cooling mass scale  $M_c$  as a parameter. Assuming that all halos start as fair samples of the universe, the global baryon fraction  $(m_d + m_b)_0 = \Omega_b/\Omega_m$ . Naively then, the only parameter of the model is the baryon density  $\Omega_b$ . In practice however, star formation complicates the interpretation. While  $\Omega_b$  controls the initial cooling of the halo, star formation can reheat the baryons once they have cooled so that the cool baryon fraction in a galaxy is less than the fraction which cooled initially (see e.g. SA). Since the adiabatic compression is due only to the cold baryons, we will call our parameter  $\Omega_{b,\text{cool}}$  and we should find that  $\Omega_{b,\text{cool}} \leq \Omega_b$ .

### 3. The Distribution of Gravitational Lens Image Separations

The distribution of image separations  $\Delta\theta$  in gravitational lenses is directly related to the redshift-averaged distribution of halos  $dn/dM$ , where the conversion depends on the halo mass, redshift, and internal structure. Given a large well-defined lens sample, the image separation distribution will be the cleanest global probe of the halo mass function because the selection of the lenses is independent of the flux or surface brightness of the baryons in the halo. Lens surveys also avoid the distinction between low-mass (galaxy) and high-mass (cluster) systems required

for any other global estimate of the mass function. Wide separation lenses (usually defined by  $\Delta\theta \geq 3''.0$ ) are created by groups and clusters of galaxies and small separation systems are created by individual galaxies. We will show, however, that a successful model of the separation distribution must correctly include both the mass scale below which the baryons significantly modify the structure of the halo and the changes in the structure of the halos produced by the cooled baryons.

We will examine the distribution of image separations of the lenses found in the Cosmic Lens All-Sky Survey (CLASS; e.g. Browne & Myers 2000) for lensed flat-spectrum radio sources. The primary CLASS survey has a nearly uniform selection function for separations from  $0''.3 \leq \Delta\theta \leq 6''.0$ , with extensions to wider separations of  $6''.0 \leq \Delta\theta \leq 15''.0$  (Phillips et al. 2000). These surveys have found 18 lenses, all with separations  $\Delta\theta < 3''.0$ . We also considered the separation distribution of all radio-selected lenses. This sample of 27 lenses is inhomogeneously selected, but includes two wider separation lenses (MG 2016+112 and Q 0957+561) and illustrates the uncertainties in the tail of the distribution. We include the angular selection function for small separation lenses, but with an outer limit of  $15''.0$  we will be able to ignore the selection function for large separation lenses.

### 3.1. The Need for Baryons

The need for baryonic processing to explain the image separation distribution is most obvious when we consider the previous attempts to compute the distribution of lens separations based only on the properties of the dark matter (e.g. Narayan & White 1988; Kochanek 1995; Wambsganss et al. 1995; Wambsganss, Cen & Ostriker 1998; Maoz et al. 1997; Keeton 1998; Mortlock & Webster 2000; Li & Ostriker 2000, Keeton & Madau 2000, Wyithe, Turner & Spergel 2000). In these models, most of which were intended only to explain the wide separation lenses, the mass function of the parent dark matter halos is calculated using the Press-Schechter (1974) theory and its extensions. Given a mass function, the lens properties are then calculated by assuming a model for the density distribution of the halos. When the models are normalized so that they predict the correct local abundance of massive clusters, they correctly predict that wide separation lenses are rare. However, they catastrophically fail to explain the distribution of smaller separation lenses.

A purely phenomenological approach based on the local properties of galaxies, by contrast, predicts the observed properties of lenses quite well (e.g. Kochanek 1996, Keeton, Kochanek & Falco 1998). These models usually combine local galaxy luminosity functions with local kinematic relations to predict the distribution of lenses assuming a constant comoving density of galaxies, although a few studies have considered the effects of number evolution and merging (e.g. Mao & Kochanek 1994; Rix et al. 1994). These models have modest difficulty explaining the largest separation lenses observed in systematic surveys (separations of  $\Delta\theta \simeq 6''.0$ ), and cannot explain the lensing effects of rich clusters.

Keeton (1998) pointed out that the origin of the problem lay in ignoring the extra physics which makes the density structure of the lenses depend strongly on the mass scale. Any model based on the mass function of dark matter halos which assumes that the density distributions of the halos vary smoothly and continuously with mass leads to predictions for the separation distribution that include far too many wide separation lenses compared to small separation lenses. Keeton (1998) demonstrated the effect by showing that using either SIS (singular isothermal spheres) or NFW density profiles for all lenses could not explain the observations. Only by introducing a baryonic cooling mass scale  $M_c$  below which the halos were modeled as SIS lenses and above which they were modeled as NFW halos could the observed properties be explained. In particular this change in structure explains why many lenses found in groups of galaxies were associated with the galaxies in the group rather than the group halo, even though the group halo had to be more massive than its component galaxies.

Porciani & Madau (2000) used this hypothesis in their models for the separation distribution of lenses and found that the mass scale below which the halos had to cool and have the SIS density profiles was  $M_c = 3.5 \times 10^{13} M_\odot$ . We shall find a similar cooling mass scale, though our model is slightly different than that of Keeton (1998) and Porciani & Madau (2000). We also show that such a mass scale is naturally predicted by the properties of halos in hierarchical structure formation models if the baryon density is near the value preferred by big-bang nucleosynthesis (e.g. O’Meara et al. 2001).

### 3.2. The Qualitative Effects of Baryons on Lensing Properties

We start by illustrating the effects of the baryons on the lensing properties of a  $M_{\text{vir}} = 10^{12} M_\odot$  halo at redshift  $z_l = 0.5$  (implying a concentration of  $c = 8$ ), spin parameter  $\lambda = 0.04$ , baryonic mass fraction  $m_d + m_b = 0.05$ , and baryonic angular momentum fraction  $j_d = 0.05$ . Fig. 1 shows the rotation curves for the initial dark matter distribution and the final matter distribution given bulge-to-disk mass ratios of  $m_b/m_d = 0.0, 0.10$  and  $0.20$ . We see the familiar boost in the circular velocity due to the disk and the compression of the dark matter (e.g. SA). The bulge supports the central rotation velocity and slightly reduces the outer rotation velocity because the angular momentum per unit mass in the disk is rising as we increase the mass of the bulge. It is instructive to note that the mass profile, angular momentum profile and rotation curve of our compressed halos are quite different from what a pure dark matter simulation would predict. In particular the rotation curve only “recovers” to the pure dark matter form at very large radius (not shown on Fig. 1).

In Fig. 1 we also show the deflection or bending angle profile  $\alpha(x)$  produced by the lens assuming it lies at  $z_l = 0.5$  and the source lies at  $z_s = 2$ . To simplify the problem we consider only the face-on lensing properties, but we should keep in mind that systems with flat disks are more efficient lenses when inclined (see Keeton & Kochanek 1998). With these parameters, the initial dark matter distribution is a sub-critical lens and can produce no multiple images of the source.

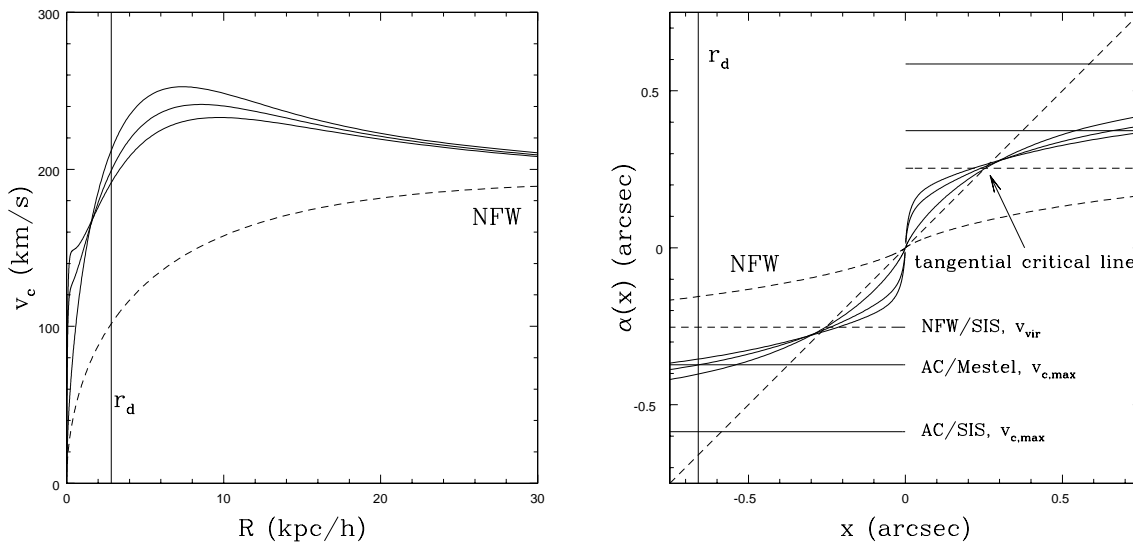


Fig. 1.— (Left) The rotation curves for  $10^{12}M_{\odot}$  halos at  $z_l = 0.5$  with concentration  $c = 8$ . The dashed curve shows the rotation curve of the initial NFW halo. The solid curves show the rotation curves found after the compression of the halo by the baryons assuming a baryonic mass fraction of  $m_d + m_b = 0.05$ , a spin parameter  $\lambda = 0.04$ , and that the disk contains all the initial baryonic angular momentum,  $j_d = 0.05$ . The three solid curves are for bulge-to-disk mass ratios  $m_b/m_d = 0$  (highest peak  $v_c$ ), 0.1 and 0.2 (lowest peak  $v_c$ ) respectively. The vertical line shows the disk scale length. (Right) The bending angles,  $\alpha(x)$ , produced by the same halos assuming a source redshift of  $z_s = 2.0$ . The dashed curve shows the deflection produced by the initial NFW halo. The solid curves show the bending angles produced after the compression of the halo by the baryons where the central deflection profile becomes steeper as we increase the bulge fraction. For comparison, the horizontal dashed lines show three simple comparison models: an SIS lens normalized by the halo virial velocity  $v_{vir}$  (NFW/SIS,  $v_{vir}$ ), an SIS lens normalized by the peak circular velocity of the compressed halo, (AC/SIS,  $v_{c,max}$ ), and a Mestel disk lens normalized by the peak circular velocity of the compressed halo, (AC/Mestel,  $v_{c,max}$ ). The tangential critical line  $x_+$  of a lens (the Einstein ring) is located at the point where the (dashed)  $45^\circ$  line intersects the bending angle, and the radial critical line  $x_-$  is located where a  $45^\circ$  line is tangent to the bending angle. An arrow points to the location of the tangential critical line of the adiabatically compressed models. The vertical solid line shows the disk scale length.

Adding the disk and compressing the dark matter pushes the lens above critical, although not by a large amount. The radial and tangential critical radii are comparable, and the lens will generally produce visible central (odd) images which are almost never seen in real systems.

The problem is that exponential disks have little density contrast between their centers and the disk scale length ( $\simeq 4h^{-1}$  kpc) while an efficient lens requires a large density contrast over this region (for a recent discussion, see Rusin & Ma 2001). The sensitivity of the lensing properties to the central density means that adding even a small bulge enormously increases the efficiency of the galaxy as a lens. For bulge-to-disk mass ratios of  $m_b/m_d = 0.05, 0.10,$  and  $0.20$  the multiple imaging cross section increases by a factors of 6, 12 and 23 compared to the model with no bulge. Moreover, the models with bulges will generally have demagnified central images, as observed in real lenses. In short, the details of the central density distribution are critical to the statistical properties of the lens, and our adiabatic compression models are inadequate for providing detailed predictions of the central density distribution.

The adiabatically compressed models are complicated, so it is of some interest to see how they compare to the far simpler SIS and face-on Mestel disk lens models. Both models have flat rotation curves and constant deflections equal to half the image separations, but if normalized to the same circular velocity they produce different image separations of  $\Delta\theta_{SIS} = 4\pi(v_c/c)^2 D_{LS}/D_{OS}$  and  $\Delta\theta_{Mestel} = 8(v_c/c)^2 D_{LS}/D_{OS}$  because a thin disk requires less mass than a spherical distribution to produce the same circular velocity (see Keeton & Kochanek 1998). Because the inner rotation curves of the adiabatically compressed models are dominated by the disks, a Mestel model normalized to the peak circular velocity provides a better match to the deflections of the adiabatically compressed models than an SIS model. Using an SIS model with a circular velocity equal to the initial halo virial velocity,  $v_{vir} = (GM_{vir}/R_{vir})^{1/2}$ , also provides a good match to the deflection scale for this model. Since most of the known lenses are produced by bulge-dominated, early-type galaxies (see Keeton et al. 1998) and seem to require mass distributions very similar to the SIS model (e.g. Cohn et al. 2001), it is interesting to note that the shape of the deflection profile becomes more similar to that of the SIS model as we increase the bulge mass fraction.

### 3.3. The Image Separation Distribution and the Density of Baryons

We explore the role of the baryons in producing the observed separation distribution of gravitational lenses in four stages. First, we illustrate the problem created by ignoring the baryons. Second, we show that introducing a mass scale,  $M_c$ , below which the halos are compressed explains the observed distribution. Third, we show that the required mass scale is consistent with simple models of cooling physics. Fourth, we show that the fundamental variable controlling the separation distribution is the cosmological density of cooled baryons. Some technical details of our calculations are relegated to Appendix A.

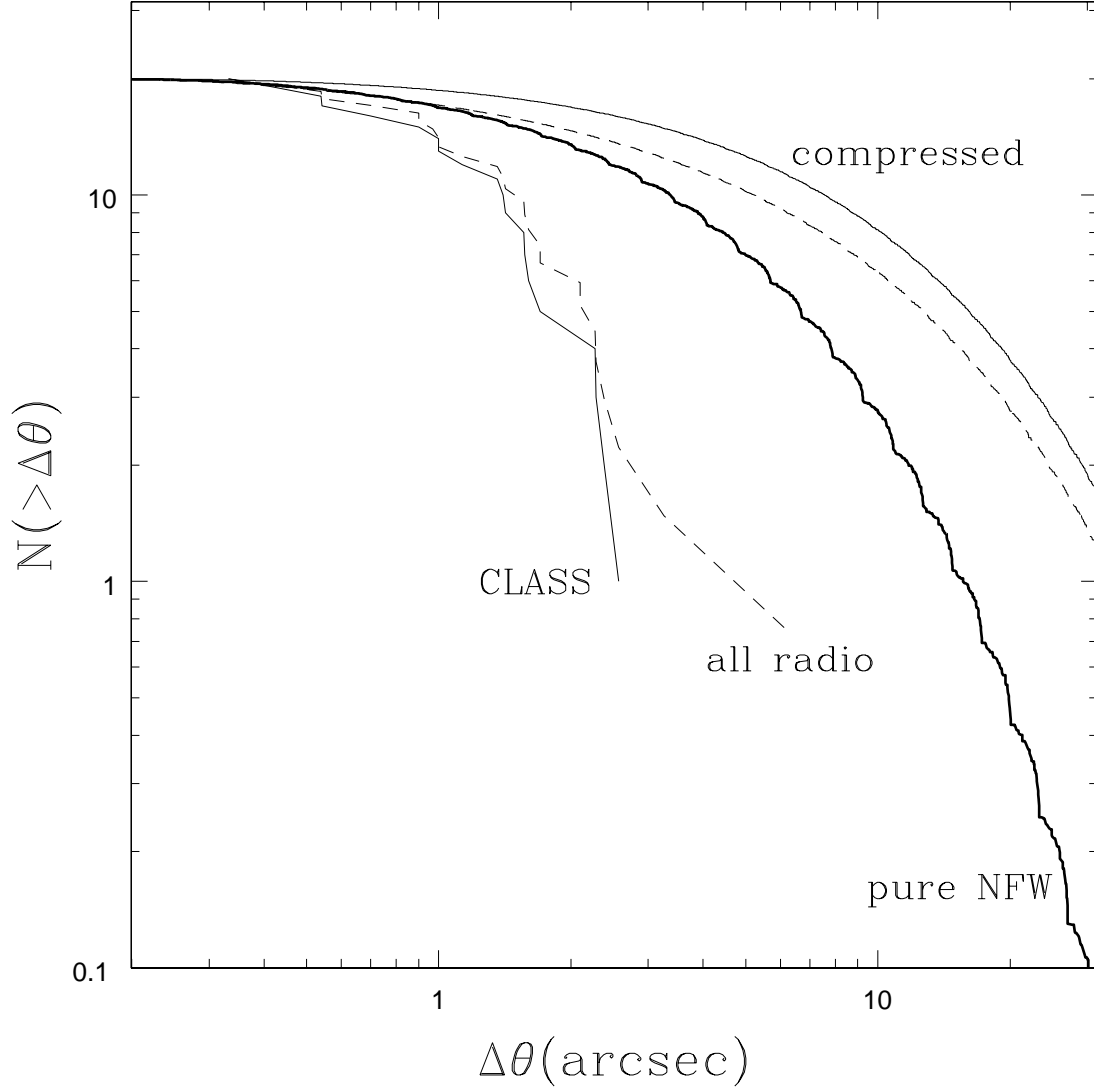


Fig. 2.— Predicted separation distributions without a cooling scale. The curves show the integral separation distribution normalized to the total number of CLASS lenses. The heavy solid line shows the distribution predicted by pure NFW models while the light solid (dashed) lines shows the distributions predicted by the adiabatic compression models with no bulge (a 10% baryonic mass fraction bulge). The wiggles in the pure NFW curve are a small discretization problem.

### 3.3.1. The Cooling Scale

The first two stages reproduce the arguments originally developed by Keeton (1998) and Porciani & Madau (2000). Consider, as a standard model, a set of halos with  $m_d + m_b = 0.05$ ,  $\lambda = 0.04$ , and  $j_d = 0.05$  with ( $m_b/m_d = 0.1$ ) and without ( $m_b/m_d = 0$ ) a bulge. If we ignore the existence of a characteristic mass scale dividing galaxies from groups and clusters, then we predict image separation distributions with far more wide separation lenses than are actually observed. The problem does not depend on the choice of model. Keeton (1998) demonstrated it using NFW and SIS models for the lenses and we illustrate it in Fig. 2 for NFW models and adiabatically compressed models both with and without a central bulge. While the low mass halos have higher NFW concentration parameters, which makes them more efficient lenses, the differences are not large enough to produce a distribution cutting off sharply at  $\Delta\theta \simeq 3''0$ .

The solution is to introduce an abrupt change in the structure of the objects at the mass scale  $M_c$  dividing galaxies and clusters. Porciani & Madau (2000) used SIS models normalized by the local properties of galaxies below  $M_c$  and NFW models above  $M_c$  and could fit the observed separation distribution given a mass scale of  $M_c = 3 \times 10^{13} M_\odot$ . We use the adiabatically compressed models below  $M_c$  and the NFW models above  $M_c$ . In our models,  $M_c$  is simply the mass at which 50% of halos have cooled based on the probability distribution defined by Eq. (9). The compressed halos have far higher cross sections per unit mass than the original NFW halos (see §3.2), leading to an increase in the fraction of small separation lenses. Fig. 3 shows the predicted distributions as a function of  $M_c$ .

If the cooling mass scale is too large,  $M_c \gtrsim 3 \times 10^{14} M_\odot$ , then we find the distribution predicted by the adiabatically compressed models without a cooling scale (Fig. 3) and cannot match the observations. If the cooling mass scale is too small,  $M_c \lesssim 10^{12} M_\odot$ , then we find the distribution predicted by the NFW models for large separations combined with a sharp peak at small separations. Only if the break is at a mass scale  $M_c \simeq 10^{13} M_\odot$  can the models reproduce the observed distribution. Interestingly, cosmological hydrodynamic simulations also find that the cooled baryon fraction reaches 50% on mass scales near  $M_c \sim 10^{13} M_\odot$  (e.g. Pearce et al. 1999).

We can quantify the goodness of fit by using the Kolmogorov-Smirnov test (e.g. Press et al. 1992) to compute the likelihood  $P_{KS}$  that the model produces a separation distribution consistent with the observations. Fig. 4 shows  $P_{KS}$  as a function of  $M_c$  for a range of models. For a fixed baryonic fraction ( $m_d + m_b$ ), the optimal value depends on the assumed structure of the low mass halos. For example, in our models  $M_c$  increases from  $M_c \simeq 5 \times 10^{12} M_\odot$  to  $M_c \simeq 10^{13} M_\odot$  when we add a  $m_b/m_d = 0.1$  bulge. By increasing the lensing efficiency of the low mass galaxies relative to the high mass galaxies (by making them more supercritical lenses), the addition of the bulge drives the estimate of the cooling mass scale upwards. An SIS model would further increase the relative lensing efficiency of the low mass galaxies, which probably explains why Porciani & Madau (2000) found a still higher break mass:  $M_c \simeq 3 \times 10^{13} M_\odot$ .

The optimal mass scale depends on the baryon fraction,  $m_d + m_b$ . With less baryons, a halo of

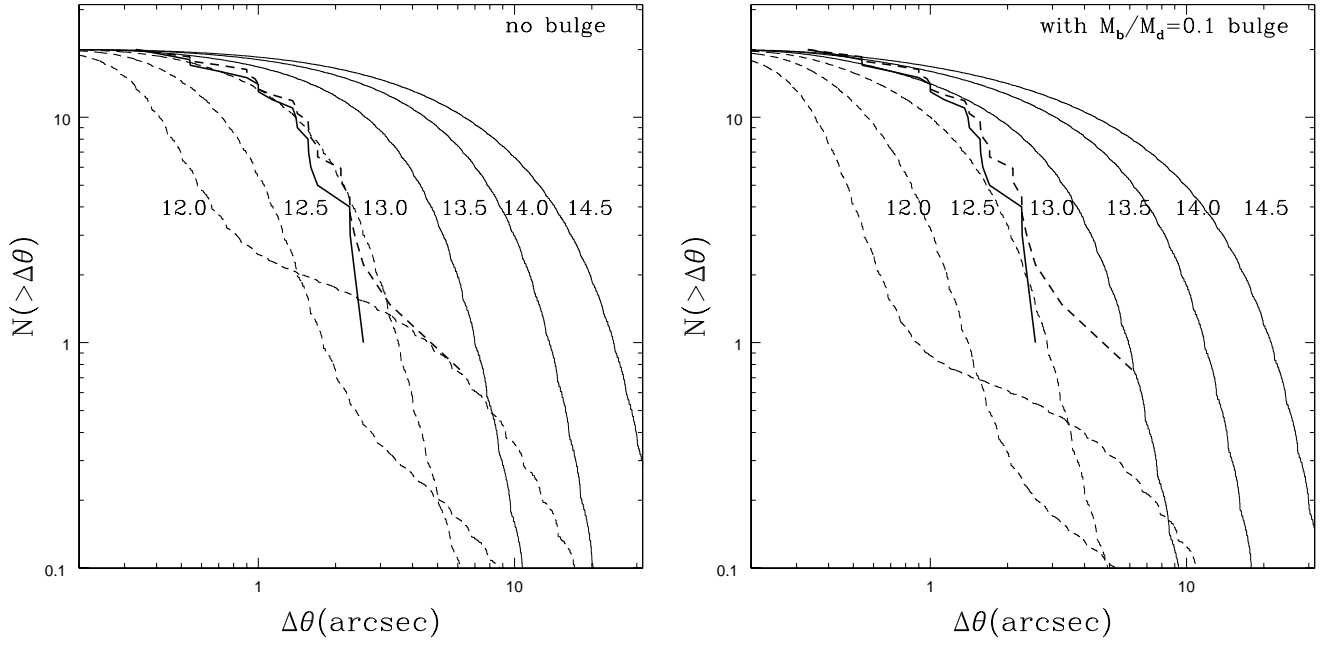


Fig. 3.— Predicted separation distributions with a cooling scale for models with a  $m_b/m_d = 0.1$  bulge (right) and without a bulge (left). The dashed curves show the distributions for  $M_c = 10^{12} M_\odot$ ,  $3 \times 10^{12} M_\odot$  and  $10^{13} M_\odot$  while the solid curves show the distributions for  $3 \times 10^{13} M_\odot$  and  $10^{14} M_\odot$ ,  $3 \times 10^{14} M_\odot$  and  $10^{15} M_\odot$ . The curves are labeled by  $\log M_c$ . The heavy solid (dashed) curve shows the observed distribution of the CLASS (radio-selected) lenses.

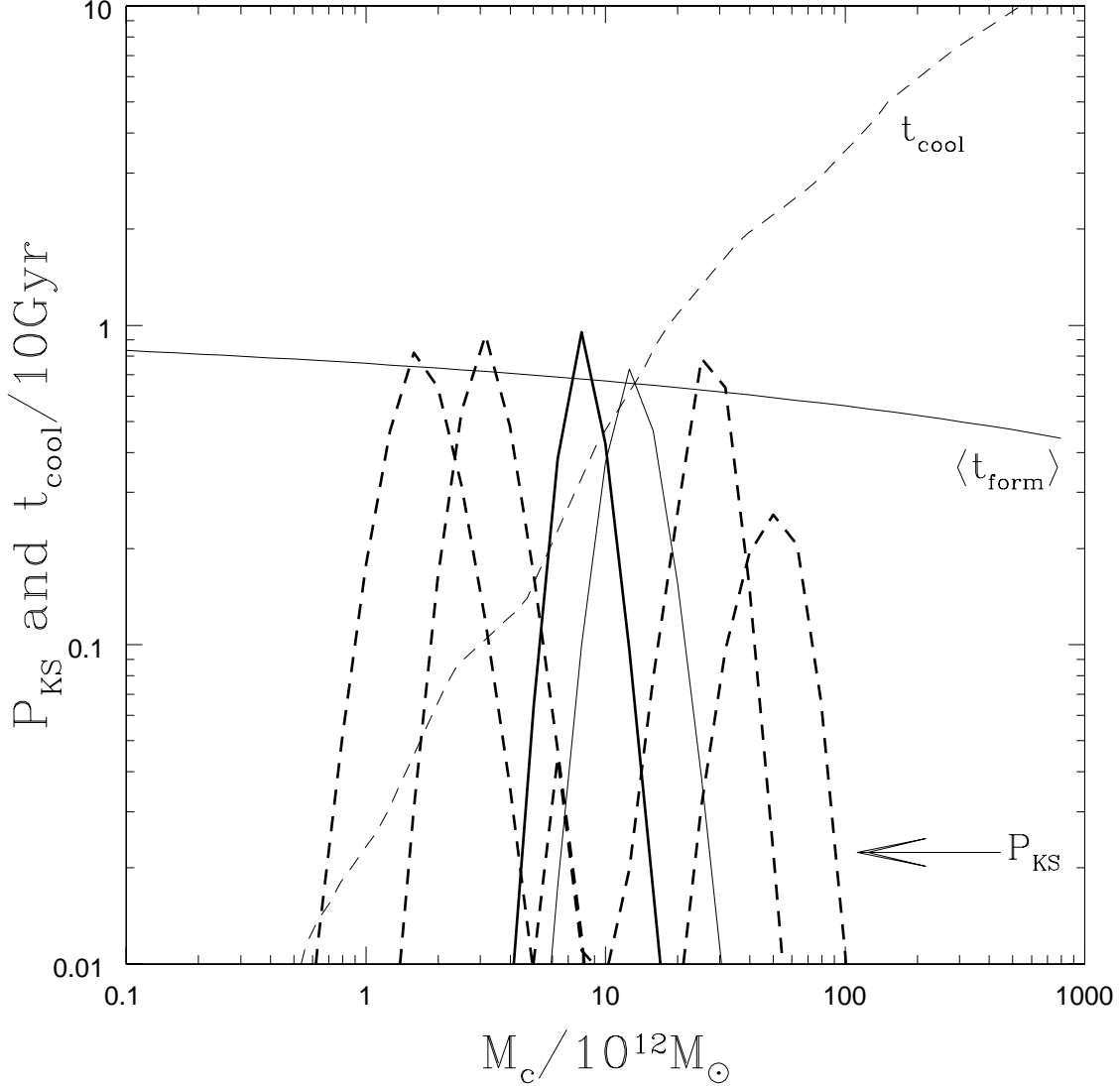


Fig. 4.— The Kolmogorov-Smirnov probability,  $P_{KS}$ , of fitting the observed separation distribution of CLASS lenses as a function of the cooling mass scale  $M_c$ . The heavy (light) solid curves indicated by the arrow show the K-S probability for models with  $m_b + m_d = 0.05$  without (with) a  $m_b/m_d = 0.10$  bulge. The heavy dashed curves show the K-S probabilities for models with lower ( $m_b + m_d = 0.01$  and  $0.02$ ) or higher ( $m_b + m_d = 0.10$  and  $0.20$ ) baryon fractions where the optimal cooling mass decreases as the baryon fraction rises. The light dashed curves show the cooling time in units of 10 Gyr for the radii enclosing 50% of the baryonic mass for the standard model. The light solid line shows the time since the average formation epoch ( $\langle t_{form} \rangle$ ) in units of 10 Gyr assuming  $h = 0.67$ .

a given mass becomes a less efficient lens producing smaller image separations, so  $M_c$  must increase to keep the observed break at a fixed image separation scale. If the baryon fraction becomes too low to significantly compress the halos ( $m_d + m_b \lesssim 0.01$ ), it becomes impossible to explain the observations. The mass scale required to explain the observations depends exponentially on the baryon fraction, with  $\log_{10} M_c/M_\odot \sim 13.6 - (m_d + m_b)/0.15$  for the models without a bulge. These trends are also shown in Fig. 4.

### 3.3.2. A Self-Consistent Model

These models, and the earlier models by Keeton (1998) and Porciani & Madau (2000), introduced the break mass as an *ad hoc* means of separating galaxies and clusters into separate lens populations. Physically this break mass is the cooling mass scale, which divides halos in which the baryons have cooled from those in which they have not, and its value should be predictable from the basic physics of cooling.

As a first step we computed the cooling times at  $z = 0$  for the radius encompassing 50% of the baryons in halos with  $m_d + m_b = 0.05$ , and compared it to the time elapsed since the average formation time of the halos. These time scales are superposed on Fig. 4. As expected, the cooling times are comparable to the time available for cooling near the mass scales required to explain the distribution of image separations. Note, however, that agreement between the cooling mass scale and the break mass required to explain the lenses depends strongly on the baryon fraction  $m_d + m_b$ . The two scales agree for our fiducial model with  $m_d + m_b = 0.05$ . For higher baryon fractions the break mass required to explain the lenses is well below the cooling mass scale, and for lower baryon fractions it is well above the cooling mass scale. Fig. 4 underestimates the problem because the cooling time also depends on the baryon fraction as  $\tau_{\text{cool}} \propto \rho_{\text{gas}}^{-1}$ . The cooling time drops when we increase the baryon fraction, which will exacerbate the discrepancies between the cooling mass and the break mass needed to explain the lenses. Thus, cooling physics makes the baryonic mass fraction,  $m_d + m_b$ , of the cooled halos the key parameter relevant to determining the distribution of image separations.

In our final models the only parameter is the halo baryon fraction  $(m_d + m_b)_0$  which should equal  $\Omega_b/\Omega_m$  for halos which are a fair sample of the universe. The cooled baryon fraction is then determined from our simple model of the cooling physics from §2.3. Figure 5 shows the separation distributions computed using our cooling model as a function  $\Omega_{b,\text{cool}}$ , where the structure of each halo is set by the adiabatically compressed models with a cooled baryon fraction of  $m_b + m_d = f_{\text{cool}}(M, z)(m_b + m_d)_0$  and  $(m_b + m_d)_0 = \Omega_{b,\text{cool}}/\Omega_m$ . The qualitative behavior of the models is similar to the more phenomenological models based on the cooling mass scale  $M_c$ . Low  $\Omega_{b,\text{cool}}$  models have difficulty cooling, making them equivalent to models with a low cooling mass scale. High  $\Omega_{b,\text{cool}}$  models cool easily, making them equivalent to models with a high cooling mass scale. Models with  $0.015 \lesssim \Omega_{b,\text{cool}} \lesssim 0.025$  agree with the observed separation distributions independent of which data we fit (CLASS lenses or all radio lenses) or the assumed

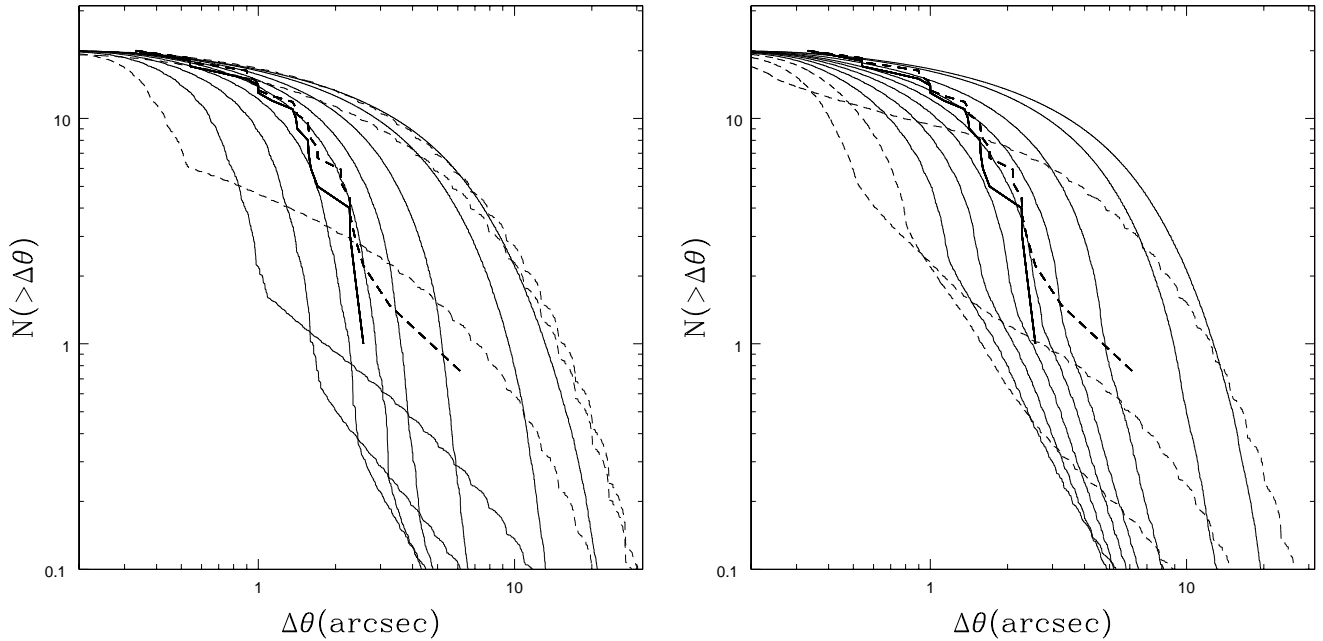


Fig. 5.— Image separation distributions as a function of  $\Omega_{b,\text{cool}}$  using models with a  $m_b/m_d = 0.1$  bulge (right) or without a bulge (left). The dashed curves show the distributions for  $\Omega_{b,\text{cool}} = 0.003$ , 0.006, and 0.009 (from right to left at large separation), and the solid curves show the distributions for  $\Omega_{b,\text{cool}} = 0.0012$ , 0.015, 0.018, 0.021, 0.024, 0.030, 0.045 and 0.060 (from left to right at large separation). The heavy solid (dashed) show the observed separation distribution of the CLASS (all radio) lenses.

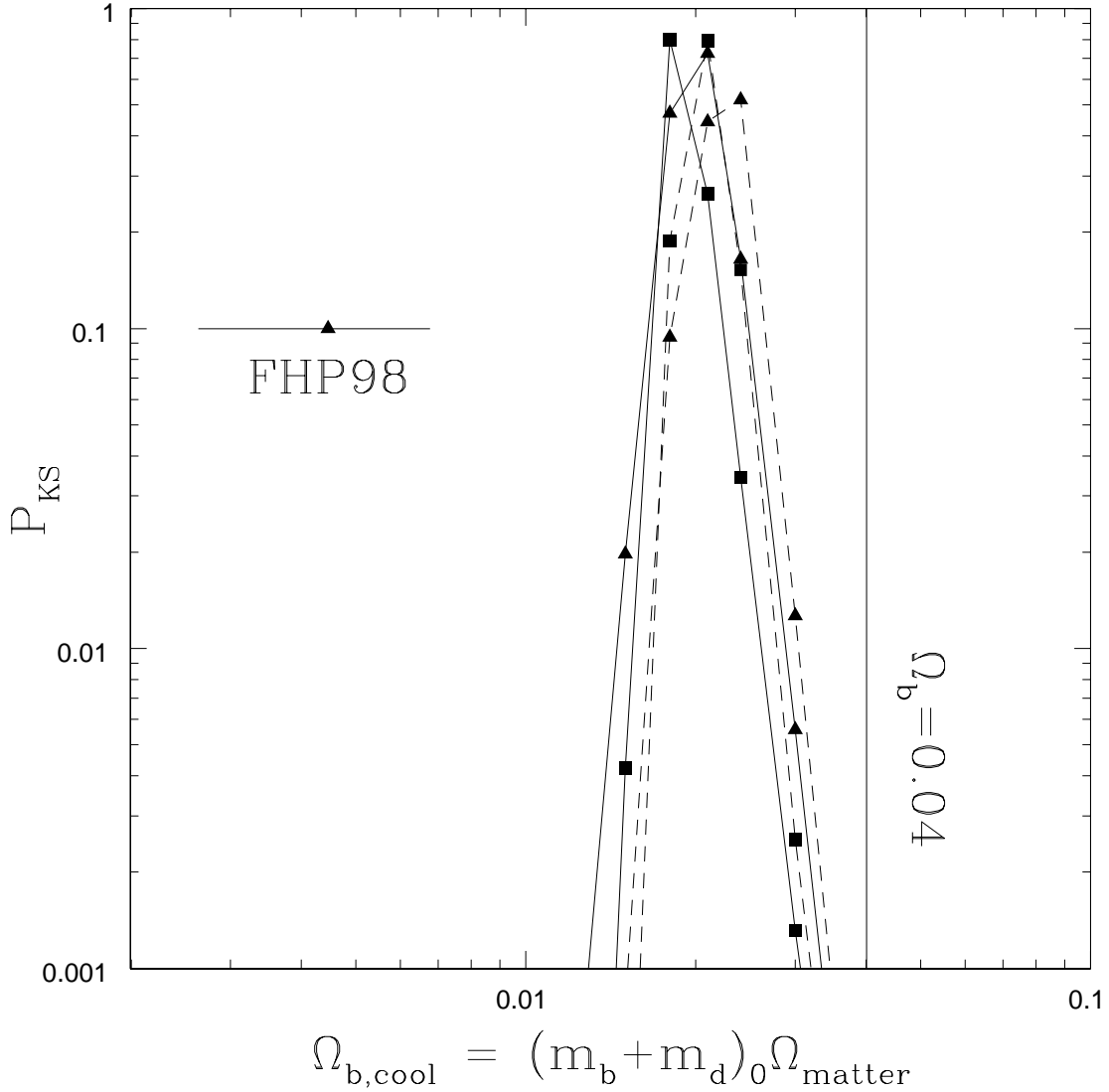


Fig. 6.— Kolmogorov-Smirnov test probability of fitting the separation distribution of CLASS lenses as a function of  $\Omega_{b,\text{cool}}$ . The squares (triangles) indicate models with no bulge (with a  $m_b/m_d = 0.1$  bulge), and the solid (dashed) lines correspond to fitting the CLASS lenses (all radio lenses). The point with horizontal error bar is the estimate by Fukugita, Hogan & Peebles (1998) for the cold baryon (stars, remnants, cold gas) content of galaxies. The vertical line marks the total baryon content in the concordance model.

density structure (with or without a  $m_b/m_d = 0.1$  bulge). The likelihoods as a function of  $\Omega_{b,\text{cool}}$  are shown in Fig. 6. The results are insensitive to modest errors in the cooling function, as raising and lowering the cooling curve by factors of two only affects the estimated baryon fraction by 20%. With the introduction of the cooling physics, there is no trivial scaling of the results for the value of the Hubble constant.

While the preferred range is less than the total baryon density  $\Omega_b = 0.04$  in the input cosmology, it significantly exceeds the estimates of  $0.0045 \lesssim \Omega_{b,\text{cool}} \lesssim 0.0068$  for the cool baryon fraction (stars, cold gas and stellar remnants) in local galaxies by Fukugita, Hogan & Peebles (1998). This discrepancy could have two explanations. First, it could be a problem in our models. The adiabatic compression models are crude approximations for the transformation of the dark matter halos by the baryons. While the estimates of  $\Omega_{b,\text{cool}}$  appear to be insensitive to changes in our assumptions, we know that the observed lens population is dominated by early-type galaxies whose baryonic density structure is very different from the assumptions used in our models. It is difficult to adequately address this possibility, since it is currently impossible to compute the final structure of a galaxy starting from the initial halo properties. Second, the accounting for the baryons in galactic halos may be incorrect. The Fukugita et al. (1998) accounting for the baryons in galaxies included only cold gas components, neglecting hot ( $10^6$  K) and warm, ionized ( $10^4$ – $10^5$  K) components. While hot gas cannot contribute the adiabatic compression of the halo, the warm components are both difficult to detect and contribute to the compression. Perhaps our best route towards understanding the detailed physical modifications of the dark matter halos by baryonic processes in hierarchical models is through simulations, but at present these have proven extremely difficult (see e.g. Navarro & Steinmetz 2000).

#### 4. The Distribution of Circular Velocities

Given our success in fitting the distributions of gravitational lens image separations, it is natural to ask whether our model agrees with estimates of the local velocity function. Global estimates of the local (circular) velocity function,  $dn/d\log v_c$ , are difficult because galaxies and clusters have very different dynamical properties and require different observational methods. We first construct a rough estimate of the local velocity function including both galaxies and clusters, and then compare it to our best self-consistent models. We stress that most of the pieces in our model have been addressed before by other authors (e.g. Turner, Ostriker & Gott 1984; Cole & Kaiser 1989; Fukugita & Turner 1991; Shimasaku 1993; Kochanek 1995, 1996; Gonzalez et al. 2000; Sigad et al. 2001) here we attempt to focus on the combination of cluster and galaxy scales to emphasize the effect of cooling in producing a change in the velocity function.

We will use the velocity function for local galaxies derived by Pahre, Kochanek & Falco (2001), which has significantly reduced systematic uncertainties compared to earlier estimates. The velocity function for groups and clusters is notoriously difficult to estimate. We will combine the X-ray temperature function estimate by Blanchard et al. (2000) with the average X-ray relation

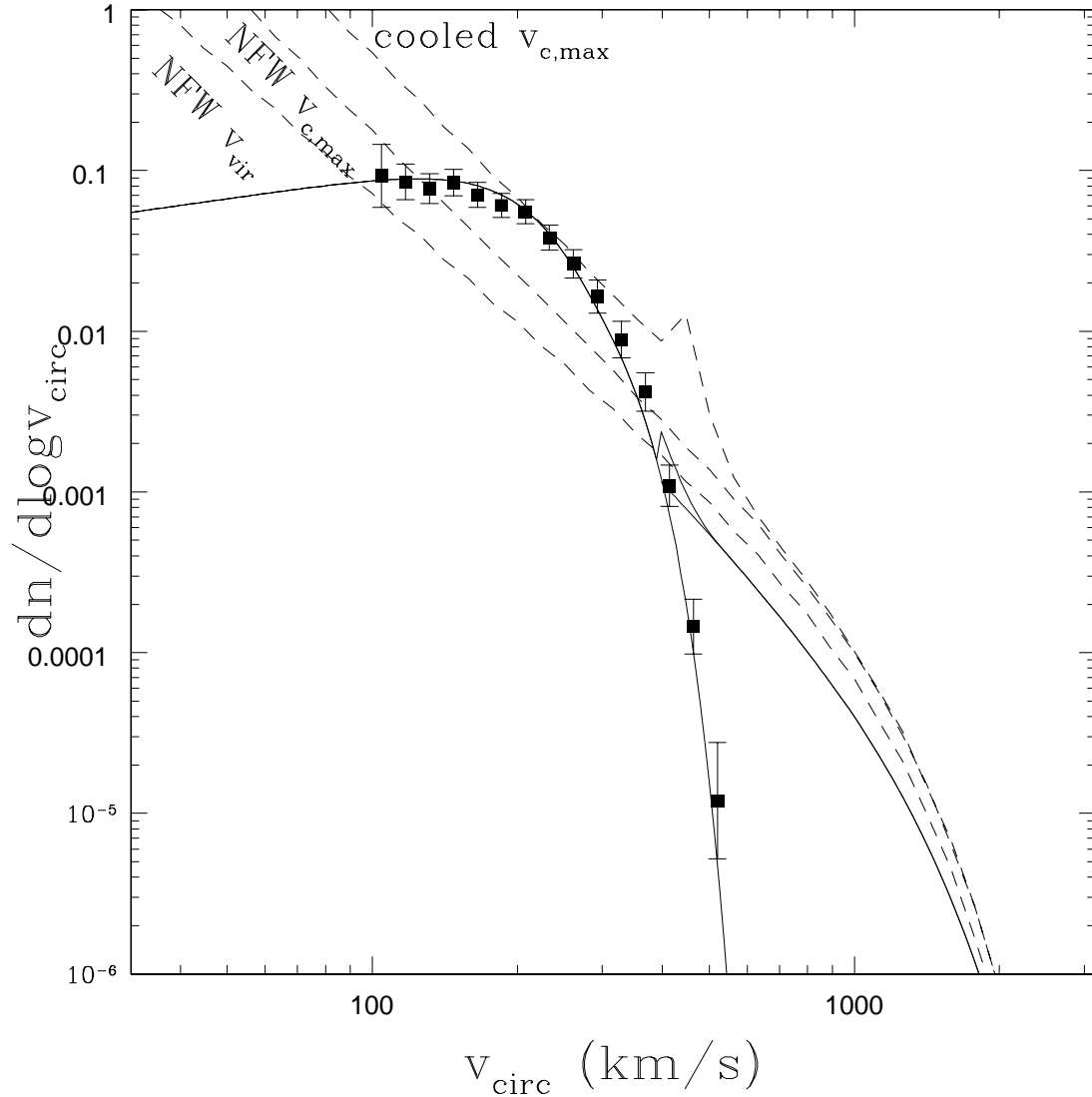


Fig. 7.— The velocity function  $dn/d\log v_c = (dn/d\log M)|d\log M/d\log v_c|$ . The solid curves show the local velocity function of galaxies (low  $v_{circ}$ ) and clusters (high  $v_c$ ) and their sum. The points are the non-parametric velocity function of galaxies. From bottom to top, the dashed curves show the velocity functions derived using  $dn/dM$  and the NFW virial velocity (labeled NFW  $v_{vir}$ ), the peak circular velocity of the NFW rotation curve (labeled NFW  $v_{c,max}$ ) and the peak circular velocity of the adiabatically compressed model (labeled cooled  $v_{c,max}$ ). We used the  $\Omega_{b,cool} = 0.018$  model with no bulge.

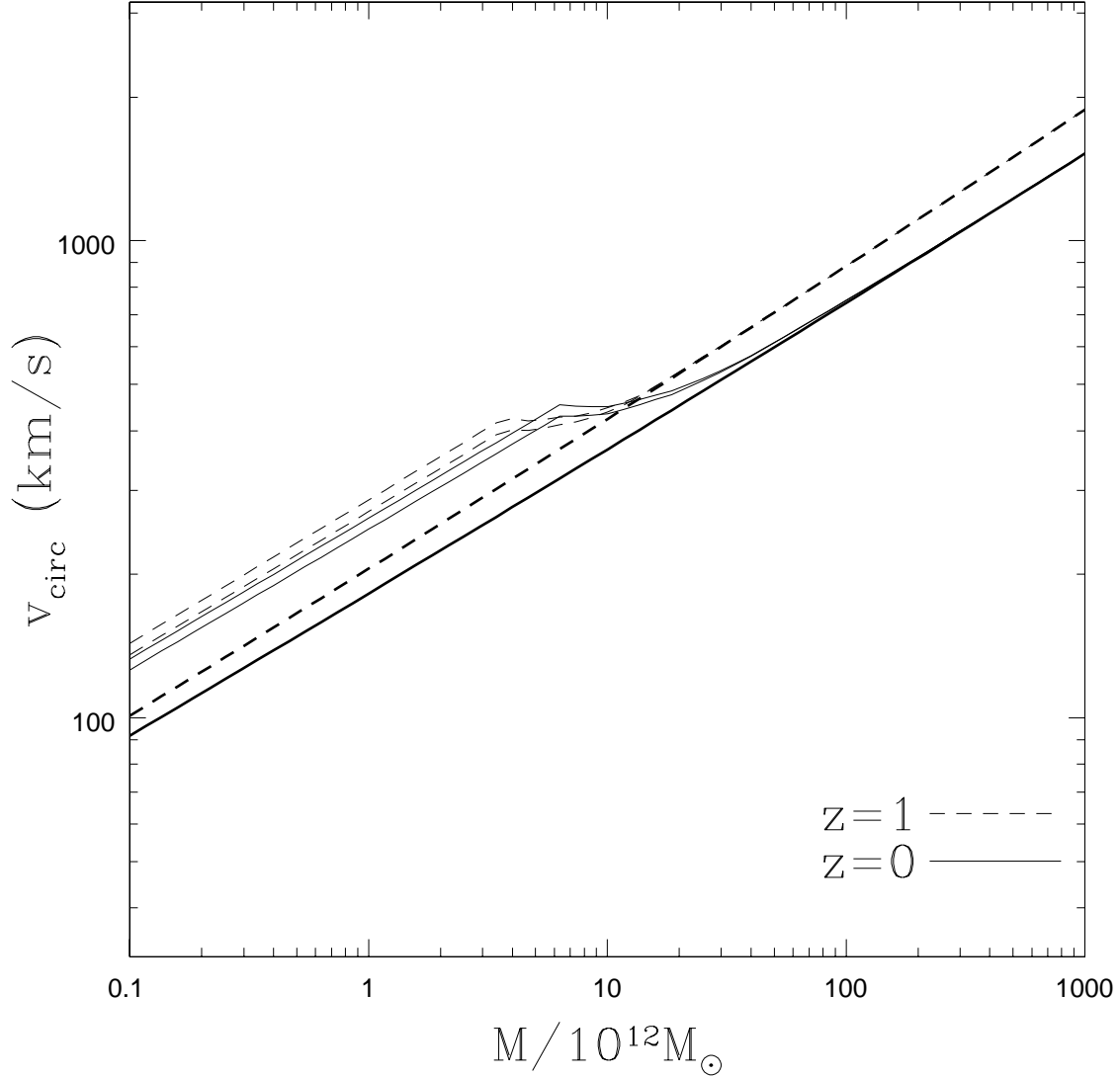


Fig. 8.— The global relation between mass and circular velocity at redshifts zero (solid) and unity (dashed). The heavy curves show the peak circular velocity of the NFW model. The light curves show the peak circular velocity including the baryonic cooling and adiabatic compression from the  $\Omega_{b,\text{cool}} = 0.018$  model. The upper light curve is the model with no bulge component ( $m_b/m_d = 0$ ) and the lower light curve is the model with a bulge ( $m_b/m_d = 0.1$ ). The bulge slightly reduces the peak rotation velocity (because it increases the angular momentum per unit mass of the disk) while making the rotation curve flatter (see §3.2).

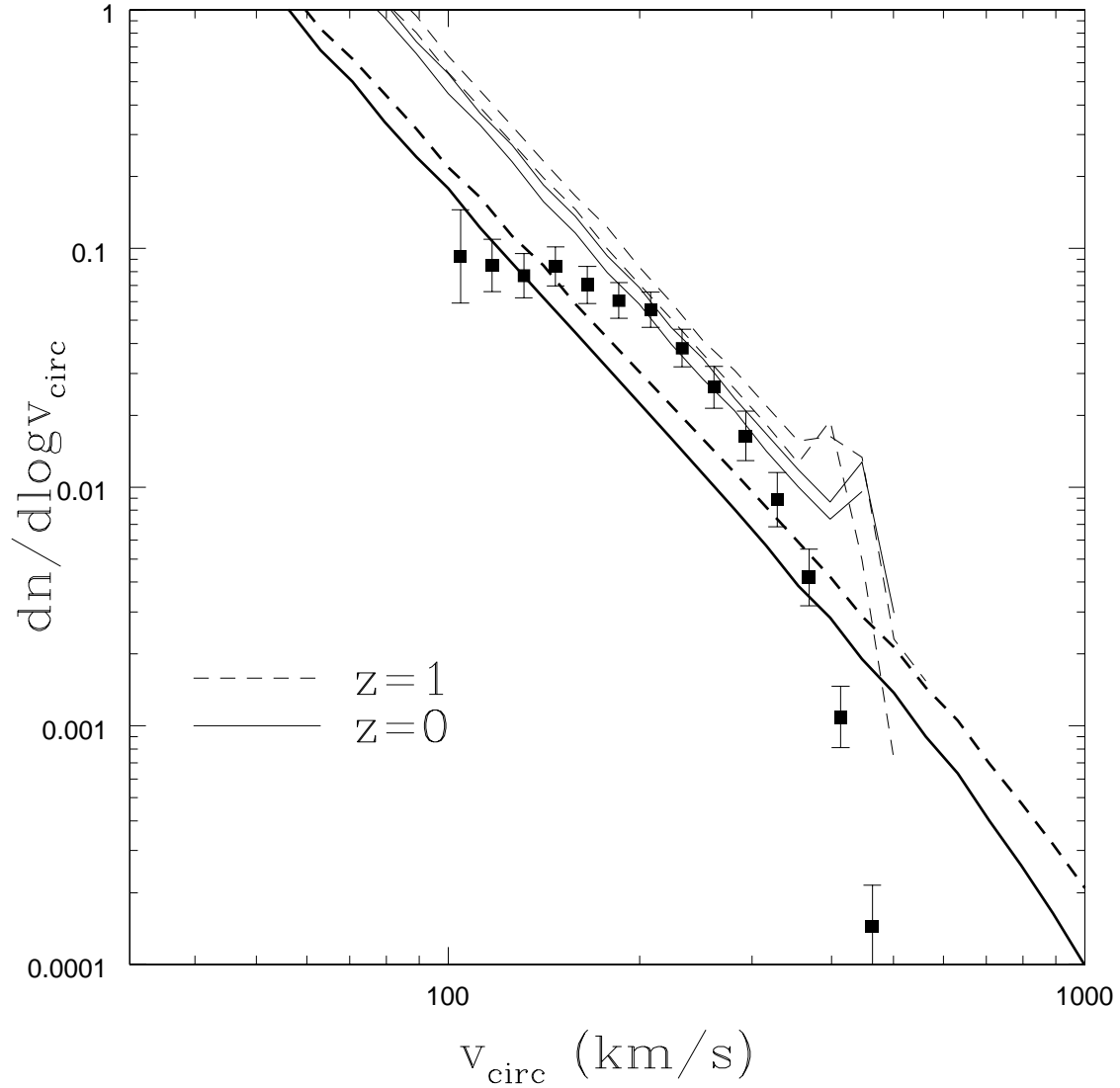


Fig. 9.— The velocity function at redshift zero (solid) and unity (dashed). The heavy curves show the results for the dark matter model. The light curves show velocity functions for halos in which at least 1/3 of the baryons have cooled in the  $\Omega_{b,\text{cool}} = 0.018$  model. The upper light curve is the model with no bulge component ( $m_b/m_d = 0$ ) and the lower light curve is the model with a bulge ( $m_b/m_d = 0.1$ ). Superposed on the distributions are the points from the velocity function of galaxies at  $z = 0$  (see text).

between the X-ray temperature and the galaxy velocity dispersion derived by Wu et al. (1999, eqn. (14)) to estimate the velocity function for groups and clusters. This velocity function estimate is nearly identical to a simple thermodynamic conversion using  $v_c = (2kT/\mu m_p)^{1/2}$  to estimate the circular velocity. There are non-trivial systematic uncertainties in our final result because of the problems in uniformly relating late-type galaxy rotation curves, early-type galaxy velocity dispersions and X-ray temperatures to a common circular velocity scale. While the upper velocity limits of galaxies are unambiguous, the lower velocity limits for groups are unknown because of the difficulty in unambiguously recognizing and counting low mass groups. For simplicity we simply truncate the cluster contribution at temperatures below 0.5 keV, which introduces a small kink in the distribution. Fig. 7 shows the estimated velocity function, which has a prominent break near  $v_c \simeq 400 \text{ km s}^{-1}$  at the boundary between the high-mass galaxies and the low-mass groups. This break in the velocity function is the local signature of the cooling mass scale, and its amplitude is far larger than any systematic uncertainties in our construction of the velocity function.

We can convert the halo mass function into the velocity function given a model relating the mass  $M$  to the circular velocity  $v_c$ . Ignoring the baryons we could use either the virial velocity of the NFW halo,  $v_{\text{vir}} = (GM_{\text{vir}}/r_{\text{vir}})^{1/2}$  or the peak circular velocity  $v_{c,\text{max}}$  of the rotation curve of the halo. A variable transformation,  $dn/d \log v_c = (dn/d \log M) |d \log M/d \log v_c|$  relates the mass function to the velocity function. Fig. 7 shows the predictions for the velocity function, and Fig. 8 shows the relationship between  $M$  and  $v_c$  for the two cases. As expected for a model normalized to match the abundance of rich clusters, the dark matter model produces a reasonable match to the velocity function of clusters given the uncertainties in the construction of the velocity function. The dark matter model catastrophically fails to match the velocity function of galaxies, grossly underpredicting the density for  $v_c \sim 200 \text{ km s}^{-1}$  and grossly overpredicting it for  $v_c \lesssim 100 \text{ km s}^{-1}$ . These discrepancies are created by the effects of the baryons in distorting the halo structure (see also Gonzalez et al. 2000).

The break in the velocity function should be reproduced by our model for the distribution of image separations. Fig. 8 shows the relationship between  $v_c$  and  $M$  for the model from §3.2 with  $\Omega_{b,\text{cool}} = 0.018$  which provided a good fit to the distribution of lens separations. For large masses, where the baryons have not cooled, the peak circular velocity matches that of the dark matter models. For small masses, all the baryons have cooled and the circular velocity curve is shifted upwards. Near  $M \simeq 10^{13} M_\odot$  there is a break in the curve between the uncompressed and fully compressed slopes. The model velocity function (Fig. 7) now has a break at the same velocity scale as the observed velocity function. The adiabatic compression shifts the more numerous low-mass halos to a higher circular velocity, bringing the density of halos with  $v_c \sim 200 \text{ km s}^{-1}$  close to that observed. The models still overpredict the density of very low mass halos,  $v_c \lesssim 100 \text{ km s}^{-1}$  probably because star formation reheats and/or disrupts low mass halos (see Gonzalez et al. 2000). These low-mass halos had no impact on the distribution of lensed image separations because the  $\sim v_c^4$  scaling of the lensing cross sections and the finite angular resolution of the surveys ( $\Delta\theta \simeq 0''.25$ ) makes the lens surveys insensitive to these mass scales. To fix this problem we would

need to adopt a similar scheme to that used in the semi-analytic models (see, e.g., SA) to fix the overabundance of low-luminosity halos: appeal to feedback to suppress star formation in these “galaxies”.

While the break in the velocity function consistent with the distribution of lens separations is located on the right velocity scale, the agreement is not perfect, principally because our model produces a peak in the velocity function at approximately  $v_c \simeq 500 \text{ km s}^{-1}$ . No similar peak is seen in the distribution of image separations because the separation distribution is smoothed by the redshift distribution of the lenses. The peak is created (mathematically) by the region near  $M = 10^{13} M_\odot$  where the  $v_c$ - $M$  relation is flat. The flat region of the the  $v_c$ - $M$  relation is produced by two problems in our model. The first is the “over-cooling” problem common to many semi-analytic models (see SA) including the Cole et al. (2000) model we used. The cooled mass and the resulting star formation predicted for halos on group mass scales are too large, leading to super-luminous galaxies which are not observed. More complicated models can significantly reduce the problem (see Cole et al. 2000). The second problem is that we assumed a deterministic relationship between mass and circular velocity by using an average formation time rather than a distribution of formation times for each halo. More complicated models which use a distribution of formation times (e.g. Cole et al. 2000; Newman & Davis 2000) would smear out the feature.

Newman & Davis (2000) proposed using the evolution of the velocity function of galaxies as a probe of the cosmological model. Our experience here suggests that uncertainties in baryonic physics relating the observed galaxy velocities to those of the “underlying” dark matter halo could impact this proposal. Fig. 8 shows the  $v_c$ - $M$  relation both today and at redshift unity. At fixed halo mass, the circular velocity of the dark matter models increases with look back time because the average density of the halos increases (Navarro, Frenk & White 1996, 1997). With the inclusion of the baryons, the evolution of the  $v_c$ - $M$  relation is considerably more complicated. First, because the time available for cooling is significantly less at redshift unity than today, the cooling mass scale evolves with redshift. In these models the cooling mass scale today is  $M \simeq 6 \times 10^{12} M_\odot$ , while at redshift unity it is  $M \simeq 3 \times 10^{12} M_\odot$ , based on the point where the  $v_c$ - $M$  relation begins to return to the dark matter relation. Because the cooling mass determines the mass of the most massive and luminous galaxies, magnitude limited studies of galaxies will be very sensitive to the evolution of the cooling scale because they are dominated by galaxies near the characteristic luminosity created by the existence of a cooling mass scale. Second, at lower masses where we might avoid problems due to the evolution of the cooling mass scale, the evolution in the circular velocity at fixed mass differs between the dark matter and adiabatically compressed models. The adiabatic compression modestly reduces the change in the circular velocity at fixed mass compared to the dark matter models. Third, the relationship between mass and circular velocity depends on the detailed of the distribution of the baryons. The models with a bulge have somewhat lower peak rotation velocities than the models without because of our choice for distributing the baryonic angular momentum (see §2.2 and §3.2).

Fig. 9 shows the evolution of the velocity function based on these different  $v_c$ - $M$  relations.

At fixed peak circular velocity, the number density of halos increases between today and redshift unity by about 25%. We also show the evolution based on the peak circular velocity distribution of halos in which at least 1/3 of the baryons have cooled. The number density at fixed circular velocity still increases, but the ratio is slightly smaller. We see that the choice of density model has reasonably strong effects, and the behavior of the velocities near the cooling scale becomes more complicated. In fact the differences between the models with and without a 10% bulge are equal to the differences created by evolution. This means that the details of the baryonic mass distribution, and the evolution of the baryonic mass distribution are at least as important as cosmology to the evolution of the velocity function of galaxies. For example, in most models of galaxy formation, the distribution of bulge parameters is itself an evolving quantity, if nothing else because the relative numbers of late-type disk galaxies and early-type, bulge-dominated galaxies evolves (see SA; for observational evidence, see, e.g. van Dokkum & Franx 2001). We have also superposed the Pahre et al. (2001) estimate of the velocity function to emphasize that our theory, even with the baryons, shows far larger differences in shape from the model predictions than the magnitude of the evolutionary effects. For these reasons we believe that the evolution of the velocity function with redshift will most likely provide crucial information about the process of galaxy formation, before it can be used to discriminate between different models for the evolution of the expansion rate.

## 5. Conclusions

The mass and velocity distributions of virialized objects include a feature, the baryonic cooling scale  $M_c$ , which divides halos which host galaxies from those which host groups and clusters. The cooling not only produces differences in morphology, but also alters the density distributions and the dynamical structure of the halos. This significantly influences the relationship between observable kinematic properties of galaxies and the properties of their “primordial” parent halo. These baryonic effects can go a long way towards reconciling theoretical predictions for the distribution of lensing separations with observations, and explaining some of the features of the galaxy and cluster velocity function.

The baryonic compression which helps support the rotation curves of galaxies also leads to an enormous increase in the cross section for the halos to be gravitational lenses, converting shallow NFW density profiles into profiles which begin to resemble the steep singular isothermal spheres preferred as models for gravitational lenses (Cohn et al. 2001). The sharp increase in the lens cross section produced by cooling the baryons leads us to expect a “break” in the separation distribution of gravitational lenses at the separation scale corresponding to the cooling mass scale. The existence of such a break was first discussed by Keeton (1998) to explain why the lenses found in systematic surveys were always associated with galaxies even when the galaxies were group or cluster members. A model incorporating an *ad hoc* break was fit to the distribution of lensing separations by Porciani & Madau (2000) and used to constrain the cooling scale to the range

$10^{13} M_{\odot}$ .

We have shown that a simple, self-consistent model based on adiabatically cooled NFW profiles can fit the observed distribution of gravitational lens separations. In this model the lenses select a cooled baryon density  $0.015 \lesssim \Omega_{b,\text{cool}} \lesssim 0.025$  independent of the lens sample we fit or our modeling of a galactic bulge. While our model is self-consistent, in the sense that it uses calculable properties of dark matter halos to convert from unmeasurable quantities to observable quantities, it is clearly simplistic at best. In particular we have neglected heating processes associated with star formation, leading to cold baryon fractions in groups and clusters which are too high and to an overestimate of the number density of low circular velocity galaxies or small separation lenses. It is gratifying that despite these shortcomings, the main features of the observations can still be understood in terms of this simple physics.

When we predict the local distribution of halos in their observed circular velocity using the same model that fit the distribution of image separations, we find that our model also has a feature in the local velocity function at the velocity scale dividing galaxies from clusters. The comparison also makes it clear that additional physics (star formation, feedback and realistic treatment of the differences between disks and bulges) and significant improvements in the cooling model are necessary to make the agreement any better than qualitative, particularly at the low  $v_c$  end of the distribution (as has been noted by e.g. Gonzalez et al. 2000).

The shortcomings of our model related to star formation and feedback could be improved by using full semi-analytic models. The density distribution on the other hand defies a simple treatment. Our “galaxies” still have very large cores, even with the bulges, and would likely predict observable central images, which are never seen in practice. To make our models more realistic we would need to have density distributions which are closer to isothermal spheres, which we would need to put in by hand as done in the semi-analytic models or the earlier lens studies of Keeton (1998) and Porciani & Madau (2000).

Finally, when we explore the evolution of the velocity function of galaxies, we find that the effects of the baryons are non-negligible. It is only at extremely large radii that the “velocity” of a galaxy provides a measure of the mass uncontaminated by baryonic processes. On smaller scales the measured quantity is related to the desired one by complicated and poorly understood physics. Further, the shape of the observed velocity function at low- $v_c$  suggests that either observational selection effects cause a drastic underestimate of low velocity systems or the efficiency of star formation is much lower in these systems than their higher velocity counterparts (or both). We do not currently understand how these effects would evolve with redshift. In addition, the amount of baryons, the fraction of the baryons which cool and its evolution, and the evolution in the average distribution of the baryons (e.g. bulge fractions) all produce changes in the velocity function that are at least as important as the evolution in the underlying mass function.

## Acknowledgements

M.W. would like to thank J. Newman and M. Davis for helpful conversations on the velocity function and extended Press-Schechter theory and J. Cohn and C. Keeton for a careful reading of the manuscript. We thank R. Croft for discussions on the warm gas fraction in galaxies. C.S.K. was supported by the Smithsonian Institution and NASA grant NAG5-8831. M.W. was supported by a Sloan Fellowship and the National Science Foundation.

### A. Simplifications to the Lens Calculations

To estimate the lensing properties of the system we assume we view the halo face on to the disk and then compute the mass  $M(R)$  enclosed by the cylindrical radius  $R$ . By doing the calculations for a face-on disk we will underestimate the total lensing cross section (see Keeton & Kochanek 1998). The bending angle of the lens is then  $\alpha_0 = 4GM(< R)/c^2R$  and the lensed images are found as the solutions of

$$u = \frac{R}{D_{OL}} \pm \alpha_0(R) \frac{D_{LS}}{D_{OS}} = x \pm \alpha(x) \quad (\text{A1})$$

where  $u$  is the angular source position,  $x = R/D_{OL}$  is the angular position of the image,  $\alpha(x) = (D_{LS}/D_{OS})\alpha_0(D_{OL}x)$  and  $D_{OL}$ ,  $D_{LS}$  and  $D_{OS}$  are angular diameter distances between the Observer, Lens and Source (see Schneider, Ehlers & Falco 1992).

As is true for any circular lens, the tangential critical line (Einstein ring) is at the solution  $x_+$  of  $1 - \alpha(x_+) = 0$  and the radial critical line  $x_-$  is at the solution of  $1 - \alpha'(x_-) = 0$ . The radial caustic lies at  $u_- = |x_- - \alpha(x_-)|$  and the multiple image cross section is  $\sigma = \pi u_-^2$ . When the source is on the radial caustic, there are two images on the critical line at  $x_-$  and an additional solution at  $x_{\text{out}}$  such that the mean magnification produced by the lens in the multiply-imaged region is  $\langle M \rangle = (x_{\text{out}}/u_-)^2$ .

For a survey limited to sources brighter than flux  $F_{\text{min}}$ , the probability of finding a lens is

$$p(F_{\text{min}}) = \int D^2 dD \int dM \frac{dn}{dM} \pi u_-^2 B(F_{\text{min}}) \quad (\text{A2})$$

where  $D^2 dD$  is the comoving volume element,  $dn/dM$  is the redshift and mass dependent halo density,  $\pi u_-^2$  is multiple imaging cross section, and  $B(F_{\text{min}})$  is the magnification bias factor. We require the magnification bias term even when we consider only the distribution of image separations because the average magnifications produced by the the models differ. We will use the Einstein ring diameter ( $2x_+$ ) to estimate the image separation  $\Delta\theta$  produced by the lens, and we compute the integral distribution in separation by appropriately adjusting the limits of the integrals in Eq. (A2).

The uncertainties in the lensing properties of the halos are dominated by the assumptions and problems in deriving the mass distributions. These make estimates of the absolute lensing

probabilities problematic. Therefore we have focused only on the relative lensing probabilities, particularly the distribution of the lenses in image separation. Because the shapes of the potentials vary widely for the different lens models, we need to include an estimate of the variations in the magnification bias between the models rather than simply computing the multiple image cross sections. It is a generic feature of lens models that when the cross section is reduced by rearrangements in the structure of the lens, the mean magnification rises. Thus the resulting increase in the magnification bias makes the probability of finding the lens change less rapidly than the cross sections (see, e.g. Kochanek 1996). We need a simple model which can rapidly estimate the effects of magnification bias. Fortunately, the magnification bias of the radio lens surveys is modest because the slope of the luminosity function for radio sources fainter than the survey flux limit is flat and the estimates will be insensitive to simplifications in the calculation.

We made two simplifications in the properties of the radio sources being lensed. First, we assumed the sources lay at a fixed redshift  $z_s = 2$  rather than integrating over a distribution of lens redshifts. Second, at that redshift we used an approximate version of the pure luminosity evolution flat-spectrum radio luminosity function from Dunlop & Peacock (1990). For  $x = P/P_c(z)$ , Dunlop & Peacock (1990) used a luminosity function of the form  $dn/d\log x = d/(x^\alpha + x^\beta)$  with  $\alpha = 0.83$  and  $\beta = 1.96$ . We approximated this form by a broken power-law,  $\rho = d/x^\alpha$  for  $x < 1$  and  $d/x^\beta$  for  $x > 1$ , to simplify the calculations of magnification bias. The approximate luminosity function differs from the original only near the knee. The break in the luminosity function lies at  $\log P_c(z) = a_0 + a_1z + a_2z^2$ , where  $a_0 = 25.26$ ,  $a_1 = 1.18$  and  $a_2 = -0.28$  and  $P$  (in units of  $\text{W Hz}^{-1} \text{ str}^{-1}$ ) is related to the flux (in Jy) by  $P = FD_0^2(1+z)^{1+\alpha}$ ,  $\alpha = 0$  is the average spectral index assumed for flat spectrum sources, and  $D_0/(1+z)$  is the angular diameter distance in an  $\Omega_m = 1$  cosmology. The density factor  $d$  will not enter our calculation, since we considered only a fixed source redshift, but it is  $d_0(dV_0/dz)/(dV/dz)$  where  $d_0$  is a constant density,  $dV_0/dz$  is the comoving volume factor in an  $\Omega_m = 1$  cosmology and  $(dV/dz)$  is the comoving volume factor in the cosmology we used for our calculation. These corrections are required to convert the Dunlop & Peacock (1990) model from the  $\Omega_m = 1$  model in which it was derived to the cosmology we are using in our calculation.

We then simplified the magnification bias calculation by assuming that the magnification probability distribution was  $P(> M) = (M_0/M)^2$  for  $M \geq M_0$  where we could estimate the minimum magnification from the mean magnification produced by the lens,  $2M_0 = \langle M \rangle$ . This approximation is exact for a SIS lens and the functional form is asymptotically correct for any lens dominated by fold caustics. By combining our approximate magnification distribution with our broken power law model for the luminosity function, we can analytically compute the magnification bias for CLASS sample.

## REFERENCES

Baugh C.M., Cole S., Frenk C.S., 1996, MNRAS, 283, 1361

- Benson A.J., et al., 2000, MNRAS, 311, 793
- Blanchard A., Sadat R., Bartlett J.G., Le Dour M., 2000, A&A, 362, 809
- Blumenthal G.R., et al., 1984, Nature, 341, 517
- Blumenthal G.R., Faber S.M., Flores R., Primack J.R., 1986, ApJ, 301, 27
- Browne I.W.A., Myers S.T., 2000, IAU Symposium 201, 47
- Bullock J.S., et al., 2000, preprint [astro-ph/9908159]
- Cohn J.D., Kochanek C.S., McLeod B.A., Keeton C.R., 2001, ApJ, in press [astro-ph/0008390]
- Cole S., et al., 1994, MNRAS, 271, 781
- Cole S., Kaiser N., 1989, MNRAS, 237, 1127
- Cole S., Lacey C.G., Baugh C.M., Frenk C.S., 2000, MNRAS in press [astro-ph/0007281]
- Dalcanton J.J., Spergel D.N., Summers F.J., 1997, ApJ, 482, 659
- Dunlop J.S., Peacock J.A., 1990, MNRAS, 247, 19
- Eke V., Navarro J.F., Steinmetz M., 2001, preprint [astro-ph/0012337]
- Fukugita M., Hogan C.J., Peebles P.J.E., 1998, ApJ, 503, 518
- Fukugita M., Turner E.L., 1991, MNRAS, 253, 99
- Gonzalez A.H., et al., 2000, ApJ, 528, 145 [astro-ph/9908075]
- Hernquist L., 1990, ApJ, 356, 359
- Jenkins A., Frenk C.S., White S.D.M., Colberg J.M., Cole S., Evrard A.E., Yoshida N., 2000, MNRAS, in press [astro-ph/0005260]
- de Jong, R.S., 1996, A&A, 313, 45
- Kauffmann G., Colberg J.M., Diaferio A., White S.D.M., 1999, MNRAS, 303, 188
- Kauffmann G., White S.D.M., Guiderdoni B., 1993, MNRAS, 264, 201
- Keeton C.R., Madau P., 2000, ApJ submitted [astro-ph/0101058]
- Keeton C.R., Kochanek C.S., Falco E.E., 1998, ApJ, 509, 561
- Keeton C.R., Kochanek C.S., 1998, ApJ, 495, 157
- Keeton C., 1998, thesis.

- Keeton C.R., Kochanek C.S., 1998, ApJ, 495, 157
- Kochanek C.S., 1995, ApJ, 453, 545
- Kochanek C.S., 1996, ApJ, 466, 638
- Kochanek C.S., Pahre M.A., Falco E.E., Huchra J.P., Mader J., Jarrett T.H., Chester T., Cutri R., Schneider S.E., 2000, ApJin press [astro-ph/0011456]
- Kitayama T., Suto Y., 1996, ApJ, 469, 480
- Lacey C., Cole S., 1994, MNRAS, 271, 676
- Lacey C., Silk J., 1991, ApJ, 381, 14
- Li L-X., Ostriker J.P., 2000, preprint [astro-ph/0010432]
- Mao S.D., Kochanek, C.S., 1994, MNRAS, 268, 569
- Maoz D., Rix H.-W., Gal-Yam A., Gould A., 1997, ApJ, 486, 75
- Mo H.J., Mao S., White S.D.M., 1998, MNRAS, 295, 319
- Moore B., et al., 1998, ApJ, 499, L5
- Mortlock D.J., Webster R.L., 2000, MNRAS, 319, 872 [astro-ph/0008081]
- Narayan R., White S.D.M., 1988, MNRAS, 231, 97P
- Navarro J., Frenk C.S., White S.D.M., 1996, ApJ, 462, 563
- Navarro J., Frenk C.S., White S.D.M., 1997, ApJ, 490, 493
- Navarro J., Steinmetz M., 2000, ApJ, 538, 477
- Newman J.A., Davis M., 2000, ApJ, 543, L11 [astro-ph/9912366]
- O’Meara J.M., et al., 2001, preprint [astro-ph/0011179]
- Ostriker J., Steinhardt P.J., 1995, Nature, 377, 600
- Pahre M.A., Kochanek C.S., Falco E.E., 2001, in preparation
- Pearce F.R., Jenkins A., Frenk C.S., Colberg J.M., White S.D.M., Thomas P.A., Couchman H.M.P., Peacock J.A., Efstathiou G., 1999, ApJ, 521, L99
- Phillips P.M., Browne I.W.A., Wilkinson P.N., Jackson N.J., 2000, IAU Symposium 201 [astro-ph/0011032]
- Porciani C., Madau P., 2000, ApJ, 532, 679

- Press W., Schechter P., 1974, *ApJ*, 187, 425
- Press W.H., Teukolsky S.A., Vetterling W.T., Flannery B.P., “Numerical Recipes”, 2nd ed., (Cambridge, UK)
- Rees M.J., Ostriker J.P., 1977, *MNRAS*, 179, 541
- Rix H.-W., Maoz D., Turner E.L., Fukugita M., 1994, *ApJ*, 435, 49
- Rusin D., Ma C.-P., 2001, *ApJin press* [astro-ph/0009079]
- Schneider P., Ehlers J., Falco E.E., 1992, *Gravitational Lenses* (Berlin: Springer-Verlag)
- Sheth R., Tormen G., 1999, *MNRAS*, 308, 119 (1999)
- Shimasaku K., 1993, *ApJ*, 413, 59
- Sigad Y., et al., preprint [astro-ph/0005323]
- Silk J., 1977, *ApJ*, 211, 638
- Somerville R., Primack J., 1999, *MNRAS*, 310, 1087
- Sutherland R., Dopita M., 1993, *ApJS*, 88, 253
- Turner E.L., Ostriker J.P., Gott J.R., 1984, *ApJ*, 284, 1
- van Dokkum P.G., Franx M., 2001, preprint [astro-ph/0101468]
- Wambsganss J., Cen R., Ostriker J.P., Turner E.L., 1995, *Science*, 268, 274
- Wambsganss J., Cen R., Ostriker J.P., 1998, *ApJ*, 494, 29
- White S.D.M., Frenk C.S., 1991, *ApJ*, 379, 52
- White S.D.M., Rees M., 1978, *MNRAS*, 183, 341
- Wu X.-P., Xue Y.-J., Fang L.-Z., 1999, *ApJ*, 524, 22
- Wyithe, J.S.B., Turner, E.L., Spergel D.N., 2000, *ApJ*, submitted [astro-ph/0007354]